Cover page

Beam interactions with Materials and Atoms

Nuclear Instruments and Methods in Physics Research, Section B.

Title of Paper: Shift of localized surface plasmon resonance by Ar–ion irradiation of Ag–Au bimetallic films deposited on Al_2O_3 single crystal

Corresponding Author with email address: Prof. Tamaki Shibayama

Phone: +81 (11) 706-6774 Fax: +81 (11) 706-6774 E-mail: shiba@qe.eng.hokudai.ac.jp

List of potential referees:

(1) Dr. Udai B. Singh

Affiliation: Inter-University Accelerator Centre, New Delhi, India

E-mail: udaibhansingh123@gmail.com

(2) Dr. Luca Repetto

Affiliation: Dipartimento di fisica, Universita di Genova, Via Dodecaneso 33, 16146 Genova, Italy

E-mail: Luca.Repetto@unige.it

(3) Prof. H. Amekura

Affiliation: National Institute for Material Science, Japan

E-mail: amekura.hiroshi@nims.go.jp

Manuscript Length Estimation Table

Number of characters (using “character count”)	23000	= A
Number of 1-column tables or figures	6	= B
Number of 2-column tables or figures	0	= C

Estimated number of printed pages =(A + 1300B + 5000C)/8500	3.6

Shift of localized surface plasmon resonance by Ar–ion irradiation of Ag–Au bimetallic films deposited on Al_2O_3 single crystals

Xuan Meng[1], Tamaki Shibayama[2,*], Ruixuan Yu[1], Shinya Takayanagi[1], and Seiichi Watanabe[2]

[1]Graduate School of Engineering, Hokkaido University, Sapporo, Hokkaido 060–8628, Japan

[2]Center for Advanced Research of Energy and Materials, Faculty of Engineering, Hokkaido University, Kita–13, Nishi–8, Kita–ku, Sapporo, Hokkaido 060–8628, Japan

Abstract

Effects of Ar–ion induced surface nanostructuring were studied using 100 keV Ar–ion irradiation of 30 nm Ag–Au bimetallic films deposited on Al_2O_3 single crystals, under irradiation fluences ranging from 5.0×10^{15} cm^{-2} to 6.3×10^{16} cm^{-2}. Scanning electron microscope was used to study the ion–beam–induced surface nanostructuring. As the irradiation fluence increased, dewetting of the bimetallic films on the Al_2O_3 substrate was observed, and formation of isolated Ag–Au nanostructures sustained on the substrate were obtained. Next, thermal annealing was performed under high vacuum at 1073 K for 2 hours; a layer of photosensitive Ag–Au alloy nanoballs partially embedded in the Al_2O_3 substrate was obtained when higher fluence irradiation ($> 3.8 \times 10^{16}$ cm^{-2}) was used. The microstructures of the nanoballs were investigated using a transmission electron microscope, and the nanoballs were found to be single crystals with a FCC structure. In addition, photoabsorption spectra were measured, and localized surface plasmon resonance peaks were observed. With increase in the irradiation fluence, the size of the Ag–Au nanoballs on the substrate decreased, and a blue–shift of the LSPR peaks was observed. Further control of the LSPR frequency over a wide range was achieved by modifying the chemical components, and a red–shift of the LSPR peaks was observed as the Au concentration increased. In summary, ion irradiation is an effective approach toward surface nanostructuring, and the nanocomposites obtained have potential applications in optical devices.

Keywords:

Ion irradiation, surface nanostructuring, Al_2O_3 substrates, Ag–Au alloy, localized surface plasmon resonance

Abbreviations:

SEM: scanning electron microscope;
TEM: transmission electron microscope;
EDS: energy dispersive spectrometer;
LSPR: localized surface plasmon resonance;
FCC: face–centered cubic.

Introduction

Physical and chemical properties of low–dimensional solid–state systems have attracted considerable attention because of their technological significance. In the past decades, metallic nanoparticles either sustained on surfaces or dispersed in dielectric matrices have been extensively studied because of their pronounced optical and electrical properties [1–8]. Most of the studies have focused on localized surface plasmon excitation, which dominates the photoabsorption spectra in the visible range. In recent years, interest in the synthesis of dielectric–matrix–based bimetallic nanocomposites has intensified because of their considerable applications in nano–optical devices, especially in localized surface plasmon resonance spectroscopy and biosensing [3, 5–8].

The synergistic control of various parameters sensitive to the localized surface plasmon resonance (LSPR) frequency, such as particle size and shape, allows the LSPR band to be tuned. Further control of the LSPR frequency over a wide range has been achieved through the use of bimetallic nanoparticles fabricated in the form of an alloy of two metals. The resulting LSPR frequency typically lies between that of the two pure components, depending on the relative amounts of the two components. To date, several types of bimetallic nanoparticles have been synthesized [9–11]. In particlular, the combinations of Au and Ag are interesting because of their composition–sensitive optical properties. In addition, complete miscibility of Au and Ag can be obtained at any composition in both bulk materials and nanoparticles [12–14].

Surface–interface modification in metal–dielectric systems can be achieved using ion irradiation. Materials under ion irradiation undergo significant atomic rearrangement and this process effectively introduces surface nanostructuring on the dielectric surface

[15]. The most obvious phenomenon is the atomic intermixing that occurs at the interface separating two materials during ion irradiation. As an energetic ion penetrates a solid, it slows down by deposition energy both to the atoms and to the electrons of the solid. During the nuclear collision, target atoms are displaced from their lattice sites. When the high energy collisions occurs near the interface, the target atoms recoiled forward and resulted in the transport of atoms, which is known as recoil mixing. In addition to recoil mixing, multiple displacements of target atoms resulting from a collision cascade surrounding the ion track happens, producing secondary recoil atom displacements, and this process is commonly referred as cascade mixing. As the irradiation fluence increases, a continuous mixed layer is formed at the interface, and consequently improving the adhesion of deposited metal films on insulating substrate. Therefore, ion beam mixing attracts much attention for their ability to produce ion modified materials with higher solute concentrations at lower irradiation fluences than can be achieved with conventional high–fluence implantation techniques. At the same time, the energy deposition for the energetic ion can effectively induce mass transfer and result in irradiation–enhanced diffusion [16–22]. This diffusion will lead to the lateral transport of metal atoms, and therefore the spinodal dewetting of thin metal films [21].

Here we report a remarkable “ion irradiation and subsequent annealing” technique, which is a top–down approach in comparison to chemical methods [10, 11]. Previously, we have synthesized single–layer gold nanoballs with a narrowed size distribution which were partially embedded in SiO_2 glass [22]. In this study, an Ar–ion irradiation process was adopted for the synthesis of gold–silver bimetallic nanoballs on Al_2O_3 substrates.

Experimental Procedure

Ion irradiation induced surface nanostructuring of Ag–Au bimetallic films with various molar ratios deposited on Al_2O_3 substrates was performed, and the tunable plasmon resonance frequency was observed. The Ag–Au bimetallic thin films were thermally evaporated on mirror polished Al_2O_3 single crystal (viz. sapphire) substrates at ambient temperature by electrically heating the Ag and Au source under a 6.0×10^{-5} Torr vacuum. The film thickness was verified to be 30 nm using a cross–sectional transmission electron microscope (TEM; JEOL JEM–2010F). After deposition, the surface morphology was analyzed using a field–emission scanning electron microscope (SEM; JEOL JSM–7001FA).

For the $Ag_{(40\%)}$–$Au_{(60\%)}$ mixture deposited on the Al_2O_3 substrates, irradiations with 100 keV Ar ions at ambient temperature with fluences of 5.0×10^{15} cm^{-2}, 1.0×10^{16} cm^{-2}, 3.8×10^{16} cm^{-2}, 4.5×10^{16} cm^{-2}, 5.2×10^{16} cm^{-2}, and 6.3×10^{16} cm^{-2} were performed to study the fluence dependence. Energies of the ions were chosen such that the range is wider than the thickness of the bimetallic layer, as calculated using the SRIM 2011 code [23]. Ar–ion irradiation on the specimen was performed using the 400 keV ion accelerator at High Voltage Electron Microscope Laboratory, Hokkaido University [24]. A low pressure of 10^{-3} Pa was maintained inside the irradiation chamber by a turbo–molecular pump. To ensure uniform irradiation, Ar–ion beam was scanned and the current was maintained at approximately 1.5 μA cm^{-2}. To investigate the chemical component dependence, Ar–ion irradiations of Ag–Au bimetallic films with molar ratios of 0.0:1.0, 0.2:0.8, 0.4:0.6, 0.8:0.2, and 1.0:0.0 on Al_2O_3 substrates were also performed to a fluence of 6.3×10^{16} cm^{-2}. After the ion irradiation, bimetallic nanoballs with

Au:Ag molar ratios of 0.0:1.0, 0.37:0.63, 0.49:0.51, 0.65:0.35, and 1.0:0.0 were synthesized due to the preferential sputtering effects under Ar ion irradiation. Optical absorption spectra were recorded over a wavelength range of 300–800 nm on a spectrophotometer (JASCO V–630) with a spectral bandwidth of 1.5 nm, and SEM observations were conducted to examine the surface modifications. The surface elemental concentration was evaluated using the SEM coupled with an energy–dispersive spectrometer (EDS). For the specimen irradiated to a fluence of 1.0×10^{16} cm^{-2}, nanoscale mapping of the surface chemical concentration was obtained using SEM equipped with EDS, which was operated at 6.0 keV. Thermal annealing was subsequently performed under high vacuum (4.25×10^{-5} Pa) at 1073 K for 2 hours, and SEM observation and photoabsorption spectra were collected to examine the surface morphology and optical properties of the samples. Moreover, microstructural characterization was performed using TEM operated at 200 keV. Cross–sectional TEM specimens were prepared using a precision ion polishing system (PIPS; JEOL AT–12310), and ion milling was performed using a cold stage to avoid undesired thermal modification of the samples. Liquid nitrogen was used to cool the samples during ion milling.

Results and Discussion

Surface nanostructuring after Ar–ion irradiation

Effects of the ion induced surface nanostructuring were studied using 100 keV Ar–ion irradiation of 30 nm Ag–Au bimetallic films deposited on Al_2O_3 substrates with the irradiation fluence increased from 5.0×10^{15} cm^{-2} to 6.3×10^{16} cm^{-2}. The ion beam induced surface nanostructures before and after irradiation were observed using SEM. For the specimen irradiated to a fluence of 1.0×10^{16} cm^{-2}, chemical concentration maps were obtained (Fig. 1). Figures1b–d show the EDS maps for alumina, silver, and gold on the sample's surface; the maps indicate that the silver and gold concentration patterns correspond to the bright network–like pattern shown in Fig. 1a. The bright contrast in the SEM images represents the retained bimetallic films on the Al_2O_3 substrates. Moreover, the surface concentration patterns of silver and gold are consistent with each other, which illustrate the nanoscale atomic mixing of Ag and Au.

With increase in the irradiation fluence, the process of bimetallic film dewetting under Ar–ion irradiation was clearly distinguished, and the formation of isolated nanostructures was finally observed. The surface of the as–deposited Al_2O_3 substrate is smooth with fine particles in a scale down to a few nanometers (inset 1 in Fig.2a), whereas the surface roughness increased and holes formed after irradiation to a fluence of 5.0×10^{15} cm^{-2} (inset 2 in Fig.2a); furthermore, the holes grew larger as the irradiation fluence increased. When the irradiation fluence increased to 3.8×10^{16} cm^{-2}, partially connected nanoscale islands formed (inset 3 in Fig.2a). Finally, isolated nanoscale islands formed on the surface when the irradiation fluence reached 6.3×10^{16} cm^{-2} (inset 4 in Fig.2a). The nanoscale islands were formed because of lateral transport

of Ag and Au atoms, which is enhanced by the irradiation induced diffusion, taking into the sputtering effects [16, 17, 20–22]. Similar features of ion induced dewetting have been reported for 800keV Kr–ion irradiation of thin Pt films on SiO_2 substrates [17], 150 keV Ar–ion irradiation of thin Au films on carbonaceous substrates [20] and 100 keV Ar–ion irradiation of thin Au films on SiO_2 substrates [22]. Areal coverage of the bimetallic films was estimated for each irradiation fluence; the areal coverage decreased linearly with increasing irradiation fluence until 4.5×10^{16} cm^{-2}, and deviated from the linear tendency thereafter, as shown in Fig. 2a. The reason for this slowed decrease was the small fraction of the surface area covered by bimetallic film with increasing irradiation fluence. In addition, a chemical concentration change of $Ag_{40\%}$–$Au_{60\%}$ bimetallic films under Ar ion irradiation was obtained by SEM–EDS analysis, which was induced by the preferential sputtering effects. With the increase of the irradiation fluence, the concentration of silver increases from 39.7% (as–deposited film) to 50.5% (with the irradiation fluence of 3.8×10^{16} cm^{-2}), and then reaches the stable value around 50% (Fig. 2b).

Effects of annealing on the nanostructures

The morphologies of the samples undergo notable variations upon thermal annealing, as revealed in the SEM images in Fig. 3. In particular, some major differences were detected after thermal annealing. As–deposited Ag–Au films on Al_2O_3 substrate after thermal annealing is quite different from the ion irradiated sample; relatively large nanoscale pitches with a Heywood diameter greater than 200 nm were observed (Fig. 3a). For the sample irradiated to a fluence of 5.0×10^{15} cm^{-2}, network–like bimetallic layers aggregated to form larger nanoballs with a small portion retained, (Fig.3b). When the dose exceeded 3.8×10^{16} cm^{-2}, partially connected nanoscale islands transformed into spherical nanoballs (Fig.2c and d). For each thermal annealed sample, mean diameter of these nanoballs was reproduced using a Gaussian fitting. The mean diameter was deduced as the position of the Gaussian peak, and the error was evaluated as the standard deviation of the Gaussian fitting. Figure 3 illustrates the mean diameter as a function of irradiation fluence, which shows an exponential decrease with the irradiation fluence. A detailed investigation of these nanoballs was performed using a TEM, showing the spherical nanoballs were partially embedded in the substrate (Fig. 4a). The bimetallic nanoballs embedment in the Al_2O_3 substrate can be interpreted as thermodynamic driving forces resulting from different surface energies of the particle and its substrate in relation to their particle–substrate interface energy, which can lead to a burrowing of the particles if the ion bombardment can induce effective ion–induced viscosity of the substrate [17, 25]. Even throng the crystalline sapphire has such low ion–induced viscosity that the burrowing effect can be neglected. After the extensive Ar ion irradiation (approximately above 3.8×10^{16} cm^{-2} in our study), the near surface of the sapphire became amorphous, which can be verified by the selected area diffraction

pattern in the TEM observation. A faint diffuse ring with the faded crystalline spots were observed after a irradiation fluence of 4.5×10^{16} cm^{-2} (Fig. 4b) indicating the formation of the amorphous layer. Therefore, ion irradiation induced viscosity of the amorphous Al_2O_3 layer was sufficient enough to accomplish this burrowing process. Moreover, diffraction pattern was obtained for a particular Ag–Au nanoball (Fig. 4c), showing the nanoball exhibited a FCC structure.

The above mentioned changes in the microstructure of the nanoballs on annealing, both from compositional and morphological points of view, strongly influence optical response. Figure 5 shows the photoabsorption spectra after thermal annealing of the samples irradiated from 3.8×10^{16} cm^{-2} to 6.3×10^{16} cm^{-2}. The absorbance band located at approximately 580 nm corresponds to the localized surface plasmon resonance (LSPR) peak exhibited by Ag–Au bimetallic nanoballs partially embedded in amorphous sapphire substrate [9, 12], and the LSPR bands show a progressive blue–shift. In general, the positions of the SPR peaks are closely related to the shape, size, and chemical composition of the nanoballs. As the irradiation fluence increased from 3.8×10^{16} cm^{-2} to 6.3×10^{16} cm^{-2}, the size of the Au nanoballs decreased, which is consistent with the blue shift of the LSPR peaks (inset in Fig. 5). For each sample, the spectra were measured for five times. The LSPR positions were choice as averaged values with their standard deviations shown in the inset of Fig. 5.

Ag–Au nanoballs with a tunable surface plasmon resonance frequency

Photosensitive bimetallic nanoballs with various Au:Ag molar ratios (0.0:1.0, 0.37:0.63, 0.49:0.51, 0.65:0.35, and 1.0:0.0) were synthesized using pre–determined molar ratios of mixtures of Au and Ag deposited on Al_2O_3 substrates. These samples were therefore irradiated with 100 keV Ar–ions to a fluence of 6.3×10^{16} cm^{-2}, and the surface morphology of the samples were examined using SEM. Figures 6 a–e showed the formation of nanoballs for all five sets of the investigated samples, and Fig. 6f shows the tunable characteristics of the LSPR frequency of Ag–Au bimetallic nanoballs. The surface plasmon absorption band was observed, and the wavelengths of maximum absorption were found to be red–shifted from approximately 497 nm (Ag nanoballs) to 583 nm (Au nanoballs) with increase in Au molar fraction. In addition, interband transitions induced absorption can be clearly recognized, especially for the wavelength less than 400 nm, and they are clearly separated from the resonance position of the surface plasmon peaks. However, for the pure silver and $Ag_{(63\%)}$–$Au_{(37\%)}$ samples, a superposition of two absorption bands were observed above 400 nm. The appearance of these bands can be clarified by the multipole excitation [26]. As the isolated nanostructures with larger size and irregular shapes appeared in their surface, multipole resonances were excited, resulting in more than one plasmon resonances peaks. The inset in Fig. 6 presents the maximum absorption peak plotted as a function of Au concentration. Even though broad absorption bands were observed for certain Ag–Au molar ratios, the maximum absorption peaks shifted toward longer wavelengths with increase in Au concentration. Therefore, the LSPR depended on the chemical concentration of the nanoballs on Al_2O_3 substrate, and the LSPR peaks tended to red–shift with increasing Au concentration. However, this tendency deviated from the

theoretical calculation [27] because various parameters such as nanoballs size and shape influence the LSPR peaks. Therefore, further investigation is needed to resolve this matter.

Conclusions

In this paper, the process of ion irradiation induced surface nanostructuring of Ag–Au bimetallic films on Al_2O_3 substrates was studied. The process of the dewetting of the Ag–Au films with the increase of irradiation fluence was examined by SEM. After they were thermally annealed, the nanostructures transformed into spherical nanoballs, and a blue–shift of the LSPR peaks was observed with the increase of the irradiation fluence. Dependence of the LSPR on the chemical concentration was also observed, and the LSPR peaks exhibited a tendency of red–shift with the increasing Au concentration. In summary, ion irradiation is an effective approach in surface nanostructuring and in controlling the LSPR properties of the metallic films on Al_2O_3 substrates. The application of these nanocomposites in optical devices is expected.

Acknowledgements

This study was supported partly by the Japan Society for the Promotion of Science (JSPS) Grant–in–Aid for Scientific Research (A) #21241025. Mr. Meng thanks the Chinese Scholarship Council for stipend support to conduct this study at Hokkaido University. The authors thank Prof. S. Yatsu, Mr. K. Ohkubo, Dr. Z. Yang, Dr. Y. Yoshida, and Mr. J. Wajima for their assistance in experiments and for helpful discussions.

[1] J. C. Riboh, A. J. Haes, A. D. McFarland, C. R. Yonzon, and R. P. V. Duyne, J. Phys. Chem. B, 107 (2003)1772.

[2] S. –J. Chen, F. C. Chien, G. Y. Lin, and K. C. Lee, Optics Letters 29 (2004) 1390–1392.

[3] P. K. Jain, K. S. Lee, I. H. EI–Sayed, and M. A. EI–Sayed, J. Phys. Chem. B 110 (2006) 7238–7248.

[4] L. M. Liz–Marzan, Langmuir, 22 (2006) 32–41.

[5] K. A. Willets and R. P. Van Duyne, Annu. Rev. Phys. Chem. 58 (2007) 267–297.

[6] P. K. Jain, X. Huang, I. H. El–Sayed, and M. A. El–Sayed, Plasmonics, 2 (2007) 107–118.

[7] N. Blow, Nature Methods, 6 (2009) 389–392.

[8] M. A. Garcia, J. Phys. D: Appl. Phys., 44 (2011) 1–20.

[9] D. Barreca, A. Gasparotto, C. Maragno, E. Tondello, and S. Gialanella, Journal of Nanoscience and Nanotechnology, 7 (2007) 2480–2486.

[10] R. Kuladeep, L. Jyothi, K. S. Alee, K. L. N. Deepak, and D. N. Rao, Optical Materials Express 2 (2011) 161–172.

[11] J. Sancho–Parramon, V. Janicki, M. Loncaric, H. Zorc, P. Dubcek, and S. Bernstorff, Appl Phys A 103 (2011) 745–748.

[12] L. Xu, L. S. Tan, and M. H. Hong, Applied optics 50 (2011) G74–G79.

[13] B. Karthikeyan, Spectrochimica Acta Part A, 96 (2012) 456–460.

[14] S. Kruss, V. Srot, P. A. V. Aken, and J. P. Spatz, Langnuir, 28 (2012) 1562–1568.

[15] M. Nastasi and J.W. Mayer, Materials Science and Engineering, R12 (1994) 1–52.

[16] K. Neubeck, C. –E. Lefaucheur, H. Hahn, A. G. Balogh, H. Baumann, K. Bethge, and D. M. Rück, Nucl. Instrum. Methods Phys. Res., Sect. B, 106 (1995) 589–596.

[17] X. Hu, D. G. Cahill, and R. S. Averback, J. Appl. Phys. 89 (2001) 7777–7783.

[18] S. Dhara, R. Kesavamoorthy, P. Magudapathy, M. Premila, B. K. Panigrahi, K. G. M. Nair, C. T.

Wu, K. H. Chen, and L. C. Chen, Chem. Phys. Lett. 370 (2003) 254–260.

[19] S. Budak, S. Guner, R. Amaral Micanisawa, C. Muntele, and D, Ila, Nuclear Instruments and Methods in Physics Research B, 266 (2008) 1574–1577.

[20] J. Prakash, A. Tripathi, V. Rigato, J. C. Pivin, J, Tripathi, K. H. Chae, S. Gautam, P. Kumar, K. Asokan, and D. K. Avasthi, J. Phys. D: Appl. Phys. 44 (2011) 125302.

[21] L. Repetto, B. Š. Batič, G. Firpo, E. Piano, U. Valbusa, Appl. Phys. Lett., 100 (2012) 223113.

[22] X. Meng, T. Shibayama, R. Yu, S. Takayanagi and S. Watanabe, J. Mater. Sci., 48 (2013) 920–928.

[23] J. F. Ziegler, J. P. Biersack and U. Littmark, The Stopping and Range of Ions in Solids, Vol.1, (Pergamon, New York, 1985 (new edition in 1996)).

[24] N. Sakaguchi, H. Kinoshita, S. Watanabe, Y. Sueishi, N. Akasaka, and H. Takahashi, Journal of Nuclear Materials, 382 (2008) 197–202.

[25] A. Klimmer, P. Ziemann, J. Biskupek, U. Kaiser, and M. Flesch, Phys. Rev. B **79** (2009) 155427.

[26] M. Quinten, Optical Properties of Nanoparticle Systems: Mie and Beyond (Wiley–VCH, Weinheim, 2011), p.127–132.

[27] J. Zhu, Physica E, 27 (2005) 296–301.

Figure captions

Fig. 1 Surface chemical concentration of $Ag_{(40\%)}$–$Au_{(60\%)}$ deposited on Al_2O_3 irradiated to a fluence of 1.0×10^{16} cm^{-2}: (a) SEM image of the sample, (b–d) EDS maps of aluminum, silver, and gold, respectively.

Fig. 2 (a) Dependence of the Ag–Au bimetallic film areal coverage on the irradiation fluence; the insets are SEM images (1.0×1.0 μm^2) for (1) $Ag_{(40\%)}$–$Au_{(60\%)}$ as–deposited samples and the samples irradiated at fluences of (2) 5.0×10^{15} cm^{-2}, (3) 3.8×10^{16} cm^{-2}, and (4) 6.3×10^{16} cm^{-2}. (b) Dependence of the silver concentration in Ag–Au bimetallic film on the irradiation fluence.

Fig. 3 Dependence of the nanoball diameter on the irradiation fluence after thermal annealing; the insets are SEM images (1.0×1.0 μm^2) for (a) $Ag_{(40\%)}$–$Au_{(60\%)}$ as–deposited samples and the samples irradiated at fluences of (b) 5.0×10^{15} cm^{-2}, (c) 3.8×10^{16} cm^{-2}, and (d) 6.3×10^{16} cm^{-2}.

Fig. 4 (a) Bright field cross sectional TEM image of $Ag_{(40\%)}$–$Au_{(60\%)}$ deposited on Al_2O_3 irradiated with 100 keV Ar–ions at a fluence of 4.5×10^{16} cm^{-2} and thermally annealed thereafter; (b) diffraction pattern for the Al_2O_3 substrate circled in dashed line in (a); (c) diffraction pattern for the Ag–Au alloy nanoball circled in solid line in (a).

Fig. 5 Photoabsorption spectra of the samples irradiated at fluences from 3.8×10^{16} cm^{-2} to 6.3×10^{16} cm^{-2} and thermally annealed thereafter. The inset shows the LSPR positions with their standard deviations as a function of the irradiation fluence.

Fig. 6 SEM images (1.0×1.0 μm^2) of 100 keV Ar–ion irradiation of the samples with (a) pure silver, (b) $Ag_{(80\%)}$–$Au_{(20\%)}$, (c) $Ag_{(40\%)}$–$Au_{(60\%)}$, (d) $Ag_{(20\%)}$–$Au_{(80\%)}$, (e) pure gold deposited on Al_2O_3 at a fluence of 6.3×10^{16} cm^{-2}. (f) Photoabsorption spectra of these samples after Ar–ion irradiation; the inset shows the LSPR positions as a function of the Au concentration.

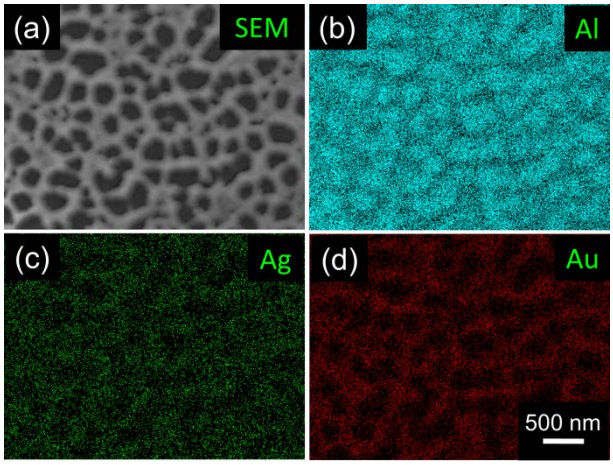

Fig. 1

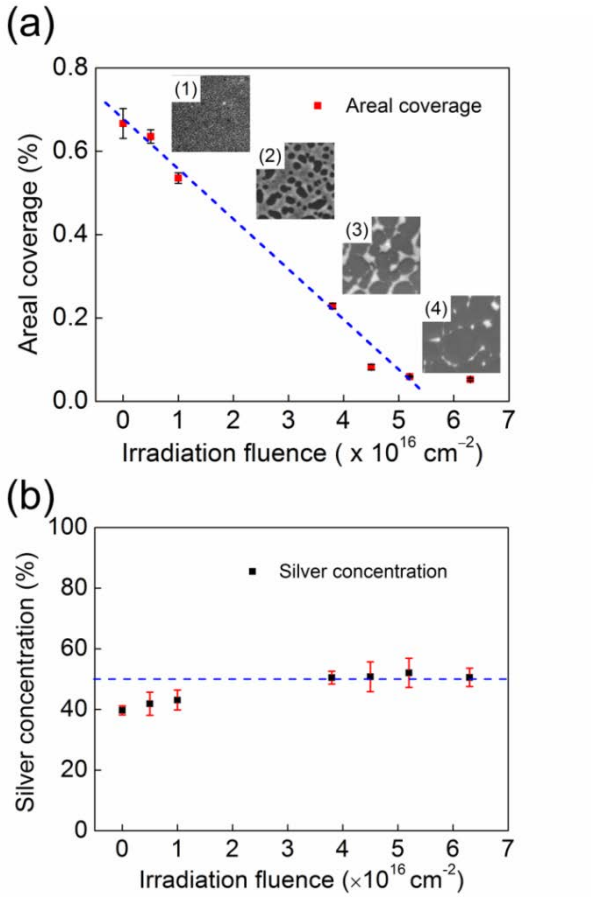
(a)
Areal coverage (%)
Areal coverage
(1)
(2)
(3)
(4)
Irradiation fluence (x 10^16 cm^-2)
(b)
Silver concentration (%)
Silver concentration
Irradiation fluence (×10^16 cm^-2)

Fig. 2

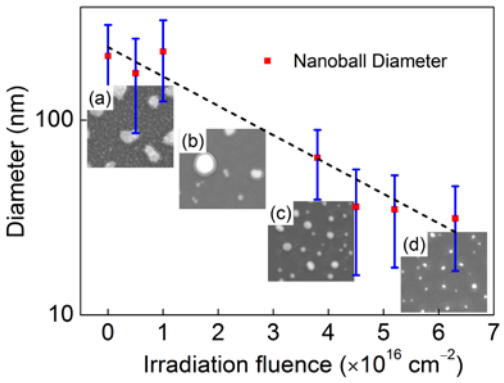
Nanoball Diameter
(a)
(b)
(c)
(d)
Diameter (nm)
100
10
0
1
2
3
4
5
6
7
Irradiation fluence (×10^16 cm^-2)

Fig. 3

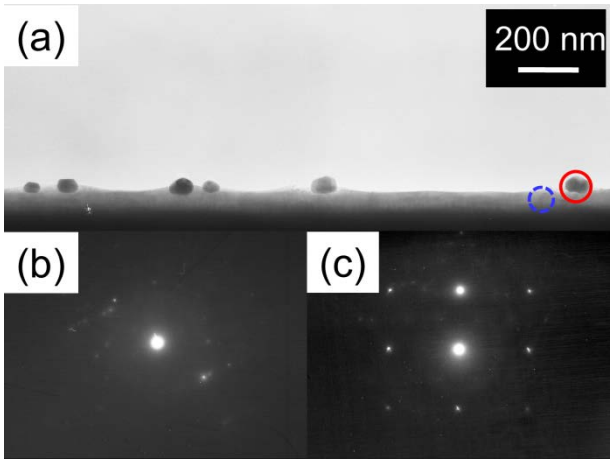

Fig. 4

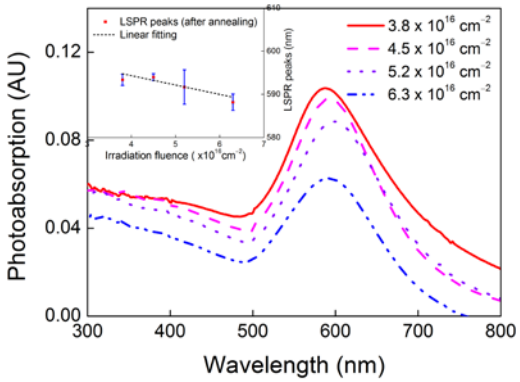
LSPR peaks (after annealing)
Linear fitting
LSPR peaks (nm)
Irradiation fluence (x10^{16}cm^{-2})
3.8 x 10^{16} cm^{-2}
4.5 x 10^{16} cm^{-2}
5.2 x 10^{16} cm^{-2}
6.3 x 10^{16} cm^{-2}
Photoabsorption (AU)
Wavelength (nm)

Fig. 5

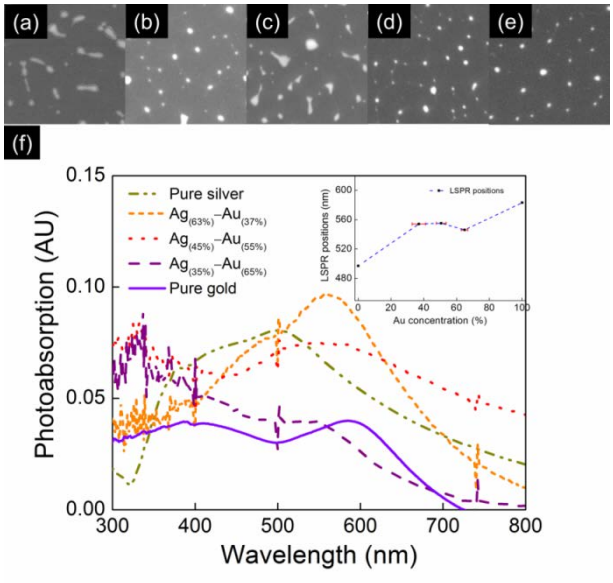
(a)
(b)
(c)
(d)
(e)
(f)
Pure silver
Ag(63%)–Au(37%)
Ag(45%)–Au(55%)
Ag(35%)–Au(65%)
Pure gold
Photoabsorption (AU)
Wavelength (nm)
LSPR positions
LSPR positions (nm)
Au concentration (%)

Fig. 6